Chemistry & Biology
Article

Structure-Guided Development of Efficacious Antifungal Agents Targeting *Candida glabrata* Dihydrofolate Reductase

Jieying Liu,[1] David B. Bolstad,[1] Adrienne E. Smith,[2] Nigel D. Priestley,[2] Dennis L. Wright,[1,*] and Amy C. Anderson[1,*]
[1]Department of Pharmaceutical Sciences, University of Connecticut, 69 N. Eagleville Road, Storrs, CT 0626, USA
[2]Promiliad Biopharma Incorporated, 950 West Fork Petty Creek Road, Alberton, MT 59820, USA
*Correspondence: dennis.wright@uconn.edu (D.L.W.), amy.anderson@uconn.edu (A.C.A.)
DOI 10.1016/j.chembiol.2008.07.013

SUMMARY

Candida glabrata **is a lethal fungal pathogen resistant to many antifungal agents and has emerged as a critical target for drug discovery. Over the past several years, we have been developing a class of propargyl-linked antifolates as antimicrobials and hypothesized that these compounds could be effective inhibitors of dihydrofolate reductase (DHFR) from *C. glabrata*. We initially screened a small collection of these inhibitors and found modest levels of potency. Subsequently, we determined the crystal structure of *C. glabrata* DHFR bound to a representative inhibitor with data to 1.6 Å resolution. Using this structure, we designed and synthesized second-generation inhibitors. These inhibitors bind the *C. glabrata* DHFR enzyme with subnanomolar potency, display greater than 2000-fold levels of selectivity over the human enzyme, and inhibit the growth of *C. glabrata* at levels observed with clinically employed therapeutics.**

INTRODUCTION

Continued antimicrobial drug research is critical, especially because of the increasing incidence of drug-resistant strains. As an example, systemic fungal infections are a significant and increasing cause of death and severe illness worldwide. Mortality rates due to *Candida* spp. infections were 38% between 1983 and 1986 and 49% between 1997 and 2001 (Hajjeh et al., 2004). The incidence of these infections has risen because of the increased number of immune-compromised patients. Up until the 1980s, *Candida albicans* was the primary cause of systemic candidemia infection (Hajjeh et al., 2004) and could be treated with traditional therapeutics including azole derivatives and amphotericin B. However, shifting epidemiology dictates that whereas *C. albicans* infections still represent the majority (~50%), other species of *Candida*, primarily *C. glabrata*, now cause a significant (~20%) number of bloodstream infections (Hajjeh et al., 2004; Pfaller and Diekema, 2004; Pfaller et al., 1999; Trick et al., 2002). This shift is due, in part, to the lower susceptibility of *C. glabrata* toward the azole compounds, especially the commonly used agent fluconazole. The therapeutic window to treat *C. glabrata* is even narrower because *C. glabrata* strains are also often resistant to amphotericin B. Isolates from the United States show the greatest degree of resistance to the azole compounds and amphotericin B (Pfaller et al., 2004).

Inhibitors of dihydrofolate reductase (DHFR) have been used clinically as anticancer, antibacterial, and antiprotozoal therapeutics for at least 60 years (Anderson, 2005; Bertino, 1993; Hawser et al., 2006). Because DHFR is essential to all cells, inhibitors targeting pathogenic organisms must be selective as well as potent in order to avoid complications resulting from inhibiting the human enzyme. There have been very few studies focusing on DHFR as an antifungal target. Although there has been some effort to develop inhibitors of *C. albicans* DHFR (CaDHFR) (Czaplinski et al., 1995; Kuyper et al., 1996; Otzen et al., 2004) and the crystal structure of CaDHFR (Whitlow et al., 1997, 2001) guided the development of a class of molecules (Chan et al., 1995) with some promising activity, up until now there have been no reported efforts to discover inhibitors of *C. glabrata* DHFR (CgDHFR).

Herein we report the development of a lead series of compounds that potently and selectively inhibit CgDHFR in enzyme assays as well as inhibit the growth of *C. glabrata* in culture, thus validating CgDHFR as a target. Furthermore, we report the crystal structure, derived from high-resolution diffraction data extending to 1.6 Å resolution, of CgDHFR complexed with NADPH and an initial potent lead from this series of inhibitors. The structure inspired the design and synthesis of second-generation CgDHFR inhibitors with subnanomolar potency and very high levels of selectivity toward the *Candida glabrata* enzyme. These second-generation inhibitors selectively kill the organism in culture at concentrations that mirror those of clinically used antifungal agents.

RESULTS AND DISCUSSION

Enzyme and Fungal Growth Inhibition

In prior work, we had developed a novel class of low molecular weight antifolates inspired by analyzing the structure of DHFR from a parasitic protozoan, *Cryptosporidium hominis* (ChDHFR) (Pelphrey et al., 2007). This series is characterized by a propargyl-based linker between the pyrimidine and substituted aryl ring. The propargyl linker extends the distance between the pyrimidine and aryl rings, relative to trimethoprim (TMP), allowing the aryl ring to fit more optimally in a hydrophobic pocket in the enzyme.

Table 1. Enzyme Inhibition and Antifungal Assay Results for Propargyl-Linked Inhibitors

Scaffold A

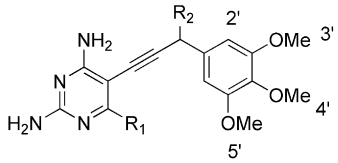

Scaffold B

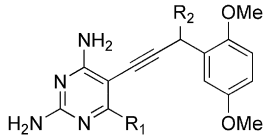

Compound	Scaffold Type	R_1	R_2	CgDHFR IC_{50} (nM)[a]	hDHFR IC_{50} (nM)	Selectivity (h/CgDHFR)	Antifungal Activity MIC (μg/ml)
TMP	-	-	-	7,300 ± 1,800	340,000	47	-
1	A	H	H	22 ± 4	1,460 ± 20	44	Inact[b]
2	A	H	CH_3	36 ± 1	1,460 ± 14	40.6	Inact
3	A	H	OH	2,700 ± 1	14,300 ± 240	5.3	328
4	A	H	OMe	450 ± 240	1,160 ± 5	2.6	Inact
5	A	CH_3	H	17 ± 1	400 ± 62	23.5	20
6	A	CH_3	CH_3	25 ± 9	1,380 ± 20	55.2	21
7	A	CH_3	OH	39 ± 5	5,710 ± 46	146	Inact
8	A	CH_3	OMe	30 ± 5	1,220 ± 7	40.7	Inact
9	B	H	H	21 ± 5	3,200 ± 53	152	71
10	B	CH_3	H	32 ± 6	1,300 ± 3	40.6	56
11	B	Et	H	8.2 ± 1	1,280 ± 15	156	78

[a] Inhibitory concentrations were measured at least three times; standard deviations are reported.
[b] Inact, not active at 2 mM (~600 μg/ml).

Although the corresponding structure of CgDHFR had not yet been determined, a comparison of the homology model of CgDHFR, based on the structure of CaDHFR (Whitlow et al., 1997, 2001), and ChDHFR suggested that these propargyl-linked inhibitors may also serve as potential antifungal lead compounds. In fact, in a homology model of CgDHFR, the hydrophobic pocket occupied by the aryl ring is displaced an additional 2 Å from the pyrimidine ring, suggesting that the extended compounds may be even more effective in CgDHFR than in ChDHFR. After expressing and purifying CgDHFR, we measured 50% inhibitory concentrations (IC_{50}) for 11 propargyl-linked compounds from our ChDHFR efforts in enzyme assays (Table 1). Many of these compounds were potent inhibitors of CgDHFR, with IC_{50} values less than 100 nM; four inhibitors (compounds **5**, **6**, **9**, and **11**) had IC_{50} values equal to or less than 25 nM. Moreover, when the propargyl compounds were assayed with human DHFR, selectivity ratios as high as 156-fold (Table 1) were observed. The IC_{50} value of TMP, 7 μM, is included in these enzyme inhibition assays as a reference and compares similarly with the value obtained with other eukaryotic DHFR species (*Candida albicans* 30 μM [Otzen et al., 2004], *Pneumocystis carinii* 12 μM [Rosowsky et al., 2002], *Cryptosporidium* 14 μM [Pelphrey et al., 2007], and *Toxoplasma gondii* 8 μM [Pelphrey et al., 2007]).

The compounds were then tested as antifungal agents in an antifungal assay against *C. glabrata*. It was exciting to discover that several of the compounds, in particular **5** and **6**, exhibit antifungal properties. The results validated the hypothesis that DHFR could be effectively targeted in a strategy to inhibit the growth of *C. glabrata*.

Crystal Structure of CgDHFR

As a first step toward the design of superior inhibitors, we determined a crystal structure of CgDHFR in complex with the most potent and selective compound from the preliminary screen, **11**, and NADPH using diffraction amplitudes that extend to 1.6 Å. The crystals belong to the tetragonal space group $P4_1$ and there are two molecules in the asymmetric unit. Results from the data collection and refinement are presented in Table 2. The overall structure of the 217 residue CgDHFR protein consists of a ten-strand central β sheet and five flanking α helices (Figure 1A). The additional two strands in the central sheet, relative to the structures of DHFR that typically have an eight-stranded β sheet, are formed from a 25 residue insert (177–202 in CgDHFR) in the sequence. These two strands form the canonical hydrogen-bond network of a β sheet with each other and with the N-terminal residues of the last strand of the standard eight-stranded central sheet. The eight-residue histidine tag used for purification formed part of the crystal packing interactions and displayed ordered electron density. There is a root-mean-square deviation (rmsd) of 0.05 Å and no significant difference between the two molecules in the asymmetric unit.

CgDHFR and CaDHFR share 85% sequence homology and can be superimposed with an rmsd of 1.62 Å over the CaDHFR Cα atoms (Figure 1B). Despite the high sequence similarity to CaDHFR, there are several key differences, including the 25 residue insert described previously. There are also two structural differences at the active site: CgDHFR has a methionine (Met33) interacting with the pyrimidine ring of the inhibitor; CaDHFR has an isoleucine in this position (Ile33). The loop containing residues

Table 2. Data Collection and Refinement Statistics

Space group	$P4_1$
Unit cell (a, b, c [Å])	a = b = 42.69, c = 230.4, α = 90, β = 90, γ = 90
Resolution (Å)	40–1.6
Completeness (%) (last shell [%])[a]	93 (92)
Unique reflections	47,676
Redundancy (last shell)	4.7 (2.9)
R_{sym} (%) (last shell [%])	6.8 (38.6)
$<I/\sigma>$ (last shell)	12.0 (2.5)
R factor/R_{free} (last shell)	0.181, 0.232 (0.234, 0.314)
Average B factor (Å^2)	24.8
Number of atoms (protein, ligands, solvent)	4,222
Number of nonhydrogen protein atoms	3,684
Number of ligand atoms	140
Number of solvent molecules	388
Rmsd bond lengths (Å), angles (°)	0.02, 2.2

[a] Highest resolution shell: 1.64–1.60 Å.

61–66 in CgDHFR is displaced 2.4 Å closer to the active site than the same loop (with residues 61–66) in CaDHFR.

Binding of Initial Lead Compound 11

Electron density for the initial lead, compound **11**, was well resolved (Figure 2A), allowing the refinement of a model of the ternary complex. Compound **11** is bound in the active site with a conserved orientation for the pyrimidine ring. The protonated N1 atom and the 2-amino group of the pyrimidine ring form hydrogen bonds with Glu32 and an ordered water molecule. Additional hydrogen bonds are formed between the 4-amino group and the backbone carbonyl oxygen atoms of Ile9 and Ile121 (Figure 2B). The C6 ethyl group points perpendicularly to the plane of the pyrimidine ring and forms limited van der Waals interactions with Leu25, Met33, and Phe36. The acetylinic linker forms van der Waals interactions with the nicotinamide ring of NADPH, Leu25, and Ile121. The dimethoxyphenyl ring fits nicely in a hydrophobic pocket composed of Met33, Ile62, Leu69, Phe66, Pro63, and Thr58. The 2′ methoxy substituent forms hydrophobic interactions with Thr58 and the 5′ methoxy substituent has interactions with Leu69, Met33, and Phe66.

Comparison with Human DHFR

The overall fold of CgDHFR is similar to that of human DHFR; however, there are several key structural differences at the active site (Figures 2C and 2D). There are four residue differences: Met33 (h:Phe31) near C6 of the pyrimidine ring; Phe66 (h:Asn64) near the aryl ring; Ile121 (h:Val115) near the pyrimidine ring; and Arg37 (h:Gln35) at the opening of the active site. The latter two residue differences are farther from the core of the active site. Importantly, the CgDHFR loop comprising residues Thr58–Phe66 is displaced 1.2 Å away from the active site, relative to the same loop comprising Thr56–Asn64 in hDHFR. The residues in the Thr58–Phe66 loop form critical hydrophobic interactions with the dimethoxyphenyl ring of the ligand. The modest selectivity (156-fold) of compound **11** potentially results from positive hydrophobic interactions between the dimethoxyphenyl ring and Met33 in CgDHFR (Phe31 in hDHFR) or repulsive van der Waals interactions between the dimethoxyphenyl ring and the loop containing Ser59–Pro61 in hDHFR, which is closer to the active site.

Docking Compound 6

Although compound **11** was the most potent and selective from the primary screen, there were several compounds with a trimethoxyphenyl ring (scaffold A) that also showed potent inhibition while exhibiting greater antifungal activity (Table 1). Specifically, compound **6** from the primary screen displays the best combination of potency, selectivity, and antifungal activity. The docked complex of compound **6** in CgDHFR revealed potential interactions of the propargyl methyl group with a pocket composed of Ile121, Thr58, and Ile62. The trimethoxyphenyl group of

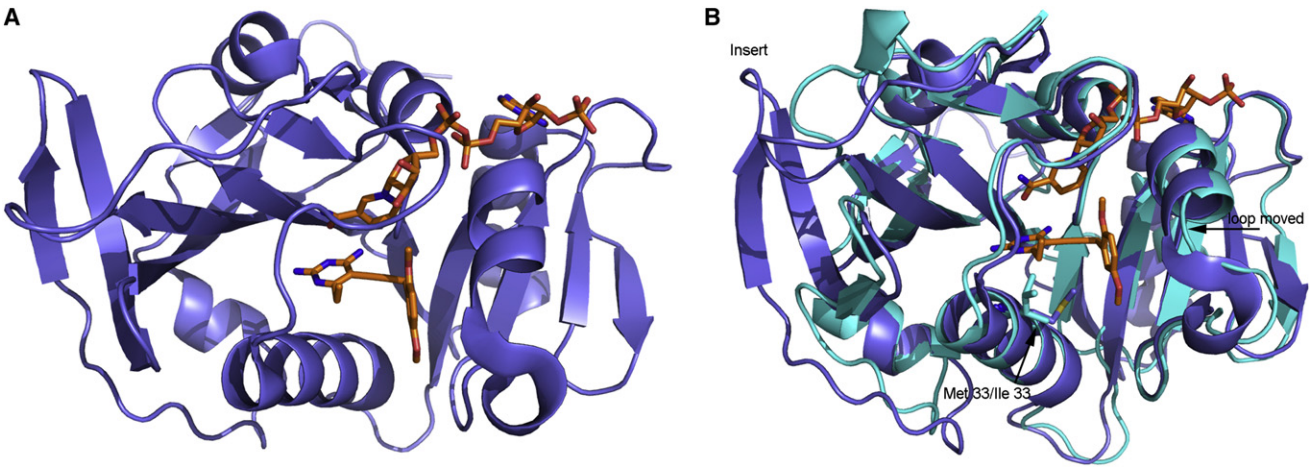

Figure 1. The Structure of CgDHFR Bound to NADPH and Compound 11

(A) Overall structure of CgDHFR. NADPH and the crystallized ligand are shown in red.

(B) CgDHFR (purple) superimposed with CaDHFR (cyan). The CgDHFR insert and loop proximal to the active site are noted.

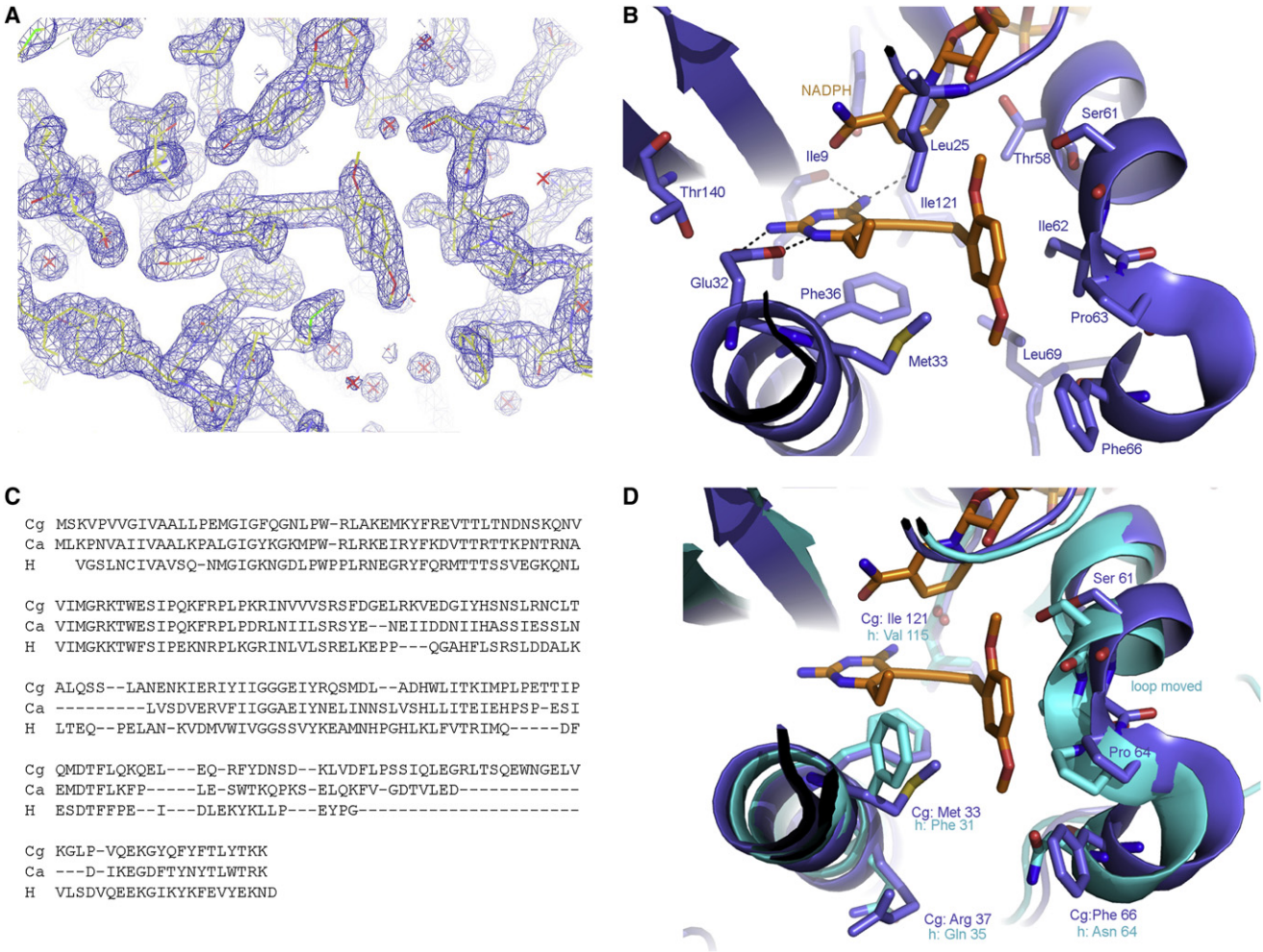

Figure 2. Potent and Selective Interactions of the Ligand

(A) Electron density for the active site and inhibitor contoured at 2σ.

(B) Interactions of compound **11** with CgDHFR, with hydrogen bonds shown as dashed lines.

(C) A sequence alignment of *Candida glabrata* (Cg), *Candida albicans* (Ca), and human DHFR (H).

(D) Comparison of CgDHFR (purple) and hDHFR (salmon). Only key residues in hDHFR at the active site are shown for clarity.

compound **6** presents a 3′ methoxy group to interact with Ser61 and Leu25, a 4′ methoxy group that has very few interactions with the protein, and a 5′ methoxy group that interacts with Ile62, Pro63, Met33, and, distally, Phe66.

Second-Generation Compounds

Several moieties of the first-generation inhibitors (compounds **1**–**11**), including a small alkyl group at the C6 position of the pyrimidine ring, the propargyl methyl group of compound **6**, and the 3′ methoxy group on the phenyl ring, yielded favorable van der Waals interactions with CgDHFR. However, additional interactions, relative to those used by compounds **11** and **6**, appeared to be available in the ligand binding pocket. It seemed that larger lipophilic moieties at the 5′ position on the aryl ring, relative to the simple methoxy group of compounds **11** and **6**, could take better advantage of the hydrophobic interactions available from Ile62, Pro63, Met33, and Phe66 (Figure 3A). A bulkier hydrophobic group at this position, designed to increase potency against CgDHFR, was also predicted to decrease potency (and increase selectivity) against hDHFR. The loop containing residues 56–64 in hDHFR is closer to the active site, and modeling suggested that it would need to relocate to accommodate steric bulk at the 5′ position of a second-generation inhibitor.

Therefore, using our high-resolution structure of CgDHFR and features of compounds **11** and **6**, second-generation inhibitors were designed to be significantly more potent and selective (Figure 3B). The series of second-generation derivatives maintain a methyl group at the C6 position of the pyrimidine, a propargyl methyl group, and the original 3′ methoxy-substituted phenyl ring. However, the new compounds also include a second aryl ring at the *meta* (5′) position of the first phenyl ring (see scaffold in Table 3). Because substituents on the second aryl ring were envisioned to project bulk toward the loop region and increase potency by interacting with residues 63–66 in CgDHFR and selectivity by interfering with residues 61–64 in hDHFR, biphenyl derivatives with methyl groups at the *meta*

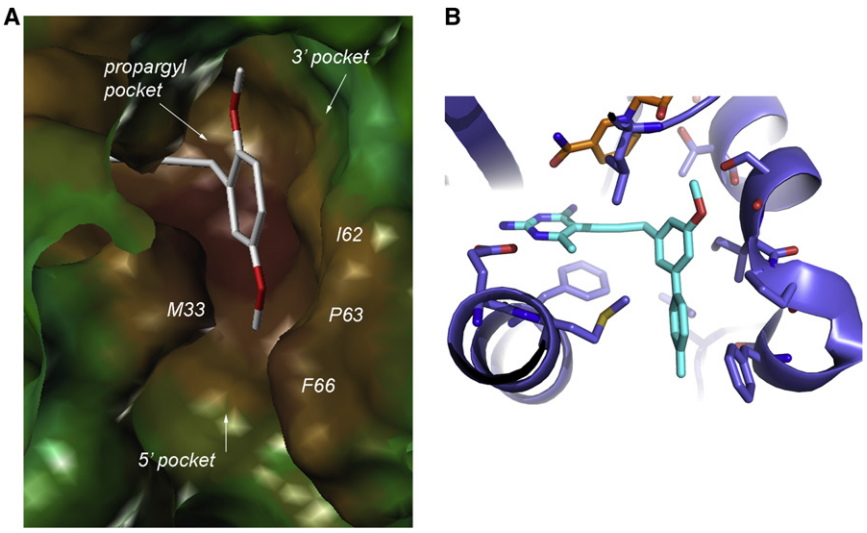

Figure 3. Structural Features Used for the Design of Second-Generation Inhibitors

(A) A surface representation of CgDHFR at the active site with compound **11** bound. The surface is colored using a gradient that extends from lipophilic (red) to neutral (green) to hydrophilic (blue). The view is the same as that shown in Figure 2B. Residues near the 5′ position of the aryl ring are labeled, as are the propargyl, 3′, and 5′ pockets. (B) A docked complex of compound **13** (cyan) in CgDHFR (purple).

(compound **12**) and *para* (compound **13**) positions on the second ring were designed.

In addition to the predicted new interactions with the enzyme, the design of the biphenyl compounds presents a facile route for synthesis. The synthesis of these compounds relies on two powerful palladium-mediated cross-coupling reactions that allow for the assembly of a potential library of ligands in a modular fashion. The original propargyl design takes advantage of a key Sonagashira coupling to join an iodinated pyrimidine with an acetylene partner (Pelphrey et al., 2007). The synthesis of the biphenyl compounds expands on this modular design to include a Suzuki coupling to install the second aryl ring. The wide availability of several diverse boronic acid coupling partners assures direct access to a wide variety of analogs. Building upon our previous methodology (Pelphrey et al., 2007), compounds **12** and **13** were synthesized for biological assay. Characterization details for compounds **12** and **13** can be accessed in Supplemental Data available online.

The second-generation compounds were tested in enzyme assays using CgDHFR and human DHFR as well as in antifungal assays (Table 3). Not only are these compounds extremely potent, with IC_{50} values in the subnanomolar range against CgDHFR, they also exhibit very strong selectivity for the fungal enzyme. Significantly, these second-generation compounds also displayed superior antifungal activity in vitro, with levels of inhibition comparable to clinically used therapeutics (Pfaller and Diekema, 2004). Evaluation of compounds **12** and **13** in human cell lines yielded an assessment of overt toxicity. We measured IC_{50} values in MCF-10 cells and then calculated selectivity ratios by dividing the IC_{50} value in the human cell line by the MIC value, the lowest concentration of compound (in micromolar units) that inhibits at least 99% of fungal cell growth (Table 3). We were very excited to find that the best lead compound is 13.5-fold selective as an antifungal agent.

SIGNIFICANCE

***Candida glabrata* is an emerging fungal pathogen that currently causes at least 20% of all candidemia infections. Unfortunately, *C. glabrata* is resistant to the majority of clinically approved antifungal agents. In this work, we describe a full cycle of structure-based drug design resulting in a lead compound effective against DHFR from *Candida glabrata*. Initial assays of a group of propargyl-based DHFR inhibitors identified two compounds with nanomolar potency against the enzyme and moderate antifungal activity. The high-resolution structure of the CgDHFR enzyme bound to one of these initial leads revealed a hydrophobic pocket near the 5′ site of the aryl ring that could be exploited for increased potency and selectivity for the pathogenic enzyme. We designed and synthesized second-generation compounds and show that they exhibit subnanomolar potency, very**

Table 3. Enzyme Inhibition and Antifungal Properties of Second-Generation Compounds

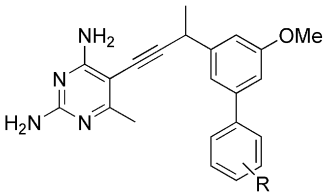

Compound	R	CgDHFR IC_{50} (nM)	hDHFR IC_{50} (nM)	Enzyme Selectivity (h/CgDHFR)	Antifungal Activity MIC	Human Cell Toxicity IC_{50} (μM)	Cellular Selectivity
12	3′, 5′ (*meta*) Me	0.55	750	1364	3 μg/ml (8 μM)	47	5.9
13	4′ (*para*) Me	0.6	1410	2350	1.5 μg/ml (4 μM)	54	13.5

high levels of selectivity, and significant antifungal activity in vitro while maintaining low mammalian cell toxicity. The structure-guided synthesis yielded 15-fold increases in potency and selectivity. The work described herein not only validates DHFR as an effective *C. glabrata* drug target but also serves to establish a lead series for further development.

EXPERIMENTAL PROCEDURES

Cloning, Expression, and Purification of CgDHFR

The gene coding for CgDHFR was amplified by PCR from *C. glabrata* genomic DNA obtained from the American Type Culture Collection (ATCC). The gene was inserted in a pET41 vector that includes a C-terminal histidine tag for nickel-affinity chromatography. *Escherichia coli* cells were transformed and the resulting plasmid was verified by sequencing. The protein was expressed in *E. coli* BL21(DE3) cells with isopropyl β-D-thiogalactoside induction. Following growth, the cells were lysed with BugBuster (Novagen) and centrifuged; the supernatant was loaded on an Ni-NTA column. The column was washed with 20 mM Tris (pH 8.0), 0.4 M NaCl and the protein was eluted using a gradient of 20 mM Tris (pH 8.0), 0.3 M NaCl, 20% glycerol, 0.1 mM EDTA, 2 mM DTT, 250 mM imidazole. Fractions containing CgDHFR were identified by SDS-PAGE, combined, and desalted using a PD-10 column with a buffer containing 20 mM Tris (pH 8.0), 20% glycerol, 0.1 mM EDTA, 2 mM DTT. The protein was concentrated to 13 mg/ml.

The gene for human DHFR (hDHFR) was amplified from cDNA obtained from ATCC, inserted in the pET41 vector, and the plasmid was verified by sequencing. The protein was expressed in *E. coli* BL21(DE3) cells and purified by nickel-affinity chromatography in a manner similar to CgDHFR.

Enzyme Assays

Enzyme activity assays were performed at 25°C by monitoring the rate of enzyme-dependent NADPH oxidation at an absorbance of 340 nm over several minutes (Joska and Anderson, 2006). All enzyme assays were performed with a single, limiting concentration of enzyme and saturating concentrations of NADPH and dihydrofolate.

Antifungal Assays

C. glabrata was stored as a suspension in 50% glycerol at −78°C. For susceptibility testing, a streak of stock culture was made on SDA agar and grown at 30°C for 48 hr. One pure colony of the test organism was recovered from the plate, suspended in appropriate media, and grown in a 5 ml shake flask culture. A sample of the shake flask culture was diluted to 1×10^5 cells/ml in media and added to 96-well test plates (100 μl per well) containing test compounds dispensed in DMSO (1 μl). Amphotericin and ketoconazole were used as controls. After an incubation period determined from the strain-specific doubling time, Alamar blue (10 μl) was added and allowed to incubate; each well was scored for dye reduction (Davey et al., 1998). The MIC value was taken as the lowest concentration of test compound that inhibits growth such that less than 1% reduction of the blue resazurin (λ_{max} 570 nm) component of the Alamar blue to the pink resorufin (λ_{max} 600 nm) was observed.

Human Cell Toxicity Assays

Adherent cell lines were maintained in Eagle's minimal essential media with 2 mM glutamine and Earle's balanced salt solution adjusted to contain 1.5 g/l sodium bicarbonate, 0.1 mM nonessential amino acids, 1 mM sodium pyruvate, 10% fetal calf serum. Fetal calf serum used in these assays was lot matched throughout. All cultures were maintained under a humidified 5% CO_2 atmosphere at 37°C, had media refreshed twice weekly, and were subcultured by trypsinization and resuspension at a ratio of 1:5 each week. Toxicity assays were conducted between passages 10 and 20. Target compound toxicity was measured by incubating the test compound with the cells for 4 hr, washing the cells, and finally treating the cells with Alamar blue. After 12–24 hr, the fluorescence of the reduced dye was measured. Fluorescence intensity as a function of test compound concentration was fit to the Fermi equation to estimate IC_{50} values.

Crystallization

CgDHFR was incubated with 1.5 mM NADPH and 1 mM compound **11** for 2 hr at 4°C. Suitable crystals (0.2 mm each side) were grown using the hanging-drop vapor-diffusion method and by mixing equal volumes of protein:ligand with 0.1 M Tris (pH 8.5), 30% PEG 4000, 0.2 M $MgCl_2$. Before flash-cooling, the crystals were transferred to a solution containing the crystallization mix and 15% glycerol. All diffraction data were measured at 100K. The initial data set was measured using an Oxford Excalibur diffractometer and processed using CrysAlis software. The high-resolution data set was measured at beamline X25A at Brookhaven National Laboratory using an ADSC CCD detector and processed with HKL2000 (Otwinowski and Minor, 1997). Data processing and refinement statistics are reported in Table 2.

Structure Determination

The structure of CgDHFR was solved by molecular replacement using the program Phaser (Read, 2001), a model of *C. albicans* DHFR (Whitlow et al., 1997) (Protein Data Bank ID code 1M79) as a search probe, and the data obtained on the Oxford system. The molecular replacement solution was used as initial phase information for the high-resolution data. Electron density maps were inspected and models were built using Coot (Emsley and Cowtan, 2004). The model was refined using Refmac5 (Murshudov et al., 1997) in the CCP4 suite. Water molecules were added automatically using functionality within Coot. The model shows good agreement with the Ramachandran plot (98.2% residues in favored regions, 1.8% in allowed regions, and no residues in disallowed regions). Figures were prepared using PyMOL (http://www.pymol.org/).

ACCESSION NUMBERS

The structure of CgDHFR:NADPH:2,4-diamino-5-(3-[2,5-dimethoxyphenyl])-prop-1-ynyl-6-ethylpyrimidine has been deposited in the RCSB Protein Data Bank under ID code 3CSE.

SUPPLEMENTAL DATA

Supplemental Data include Supplemental Experimental Data and can be found with this article online at http://www.chembiol.com/cgi/content/full/15/9/990/DC1/.

ACKNOWLEDGMENTS

The authors thank Kathleen Frey for preparing and testing compounds against hDHFR, Phil Pelphrey and Jennifer Beierlein for synthesizing compound **11**, Erin Bolstad for preparing Figure 3A, Brookhaven National Laboratory for providing access to beamline X25A, and the NIH for funding (GM067542). N.D.P. is a founder of Promiliad Biopharma, Inc.

Received: May 22, 2008
Revised: July 3, 2008
Accepted: July 23, 2008
Published: September 19, 2008

REFERENCES

Anderson, A. (2005). Targeting DHFR in parasitic protozoa. Drug Discov. Today *10*, 121–128.

Bertino, J. (1993). Karnofsky Memorial Lecture: ode to methotrexate. J. Clin. Oncol. *11*, 5–14.

Chan, J., Hong, J., Kuyper, L., Baccanari, D., Joyner, S., Tansik, R., Boytos, C., and Rudolph, S. (1995). Selective inhibitors of *Candida albicans* dihydrofolate reductase: activity and selectivity of 5-(arylthio)-2,4-diaminoquinazolines. J. Med. Chem. *38*, 3608–3616.

Czaplinski, K.-H., Hansel, W., Wiese, M., and Seydel, J. (1995). New benzylpyrimidines: inhibition of DHFR from various species. QSAR, CoMFA and PC analysis. Eur. J. Med. Chem. *30*, 779–787.

Davey, K., Szekely, A., Johnson, E., and Warnock, D. (1998). Comparison of a new commercial colorimetric microdilution method with a standard method

for in-vitro susceptibility testing of *Candida* spp. and *Cryptococcus neoformans*. J. Antimicrob. Chemother. *42*, 439–444.

Emsley, P., and Cowtan, K. (2004). Coot: model-building tools for molecular graphics. Acta Crystallogr. D Biol. Crystallogr. *60*, 2126–2132.

Hajjeh, R., Sofair, A., Harrison, L., Lyon, G.M., Arthington-Skaggs, B., Mirza, S., Phelan, M., Morgan, J., Lee-Yang, W., Ciblak, M., et al. (2004). Incidence of bloodstream infections due to *Candida* species and in vitro susceptibilities of isolates collected from 1998 to 2000 in a population-based active surveillance program. J. Clin. Microbiol. *42*, 1519–1527.

Hawser, S., Lociuro, S., and Islam, K. (2006). Dihydrofolate reductase inhibitors as antibacterial agents. Biochem. Pharmacol. *71*, 941–948.

Joska, T., and Anderson, A. (2006). Structure-activity relationships of *Bacillus cereus* and *Bacillus anthracis* dihydrofolate reductase: toward the identification of new potent drug leads. Antimicrob. Agents Chemother. *50*, 3435–3443.

Kuyper, L., Baccanari, D., Jones, M., Hunter, R., Tansik, R., Joyner, S., Boytos, C., Rudolph, S., Knick, V., Wilson, H.R., et al. (1996). High-affinity inhibitors of dihydrofolate reductase: antimicrobial and anticancer activities of 7,8-dialkyl-1,3-diaminopyrrolo[3,2-*f*]quinazolines with small molecular size. J. Med. Chem. *39*, 892–903.

Murshudov, G., Vagin, A., and Dodson, E. (1997). Refinement of macromolecular structures by the maximum-likelihood method. Acta Crystallogr. D Biol. Crystallogr. *53*, 240–255.

Otwinowski, Z., and Minor, W. (1997). Processing of X-ray diffraction data collected in oscillation mode. In Methods in Enzymology, C.W. Carter and R.M. Sweet, eds. (New York: Academic Press), pp. 307–326.

Otzen, T., Wempe, E., Kunz, B., Bartels, R., Lehwark-Yvetot, G., Hansel, W., Schaper, K., and Seydel, J. (2004). Folate-synthesizing enzyme system as target for development of inhibitors and inhibitor combinations against *Candida albicans*—synthesis and biological activity of new 2,4-diaminopyrimidines and 4′-substituted 4-aminodiphenyl sulfones. J. Med. Chem. *47*, 240–253.

Pelphrey, P., Popov, V., Joska, T., Beierlein, J., Bolstad, E., Fillingham, Y., Wright, D., and Anderson, A. (2007). Highly efficient ligands for DHFR from *Cryptosporidium hominis* and *Toxoplasma gondii* inspired by structural analysis. J. Med. Chem. *50*, 940–950.

Pfaller, M., and Diekema, D. (2004). Rare and emerging opportunistic fungal pathogens: concern for resistance beyond *Candida albicans* and *Aspergillus fumigatus*. J. Clin. Microbiol. *42*, 4419–4431.

Pfaller, M., Messer, S., Hollis, R., Jones, R., Doern, G., Brandt, M., and Hajjeh, R. (1999). Trends in species distribution and susceptibility to fluconazole among blood stream isolates of *Candida* species in the United States. Diagn. Microbiol. Infect. Dis. *33*, 217–222.

Pfaller, M., Messer, S., Boyken, L., Tendolkar, S., Hollis, R., and Diekema, D. (2004). Geographic variation in the susceptibilities of invasive isolates of *Candida glabrata* to seven systemically active antifungal agents: a global assessment from the ARTEMIS antifungal surveillance program conducted in 2001 and 2002. J. Clin. Microbiol. *42*, 3142–3146.

Read, R. (2001). Pushing the boundaries of molecular replacement with maximum likelihood. Acta Crystallogr. D Biol. Crystallogr. *57*, 1373–1382.

Rosowsky, A., Forsch, R., and Queener, S. (2002). Inhibition of *Pneumocystis carinii*, *Toxoplasma gondii* and *Mycobacterium avium* dihydrofolate reductases by 2,4-diamino-5-[2-methoxy-5-(w-carboxyalkoxy)benzyl]pyramidines: marked improvement in potency relative to trimethoprim and species selectivity relative to piritrexim. J. Med. Chem. *45*, 233–241.

Trick, W., Fridkin, S., Edwards, J., Hajjeh, R., and Gaynes, R. (2002). Secular trend of hospital-acquired candidemia among intensive care unit patients in the United States during 1989–1999. Clin. Infect. Dis. *35*, 627–630.

Whitlow, M., Howard, A., Stewart, D., Hardman, K., Kuyper, L., Baccanari, D., Fling, M., and Tansik, R. (1997). X-ray crystallographic studies of *Candida albicans* dihydrofolate reductase. J. Biol. Chem. *272*, 30289–30298.

Whitlow, M., Howard, A., Stewart, D., Hardman, K., Chan, J., Baccanari, D., Tansik, R., Hong, J., and Kuyper, L. (2001). X-ray crystal structures of *Candida albicans* dihydrofolate reductase: high resolution ternary complexes in which the dihydronicotinamide moiety of NADPH is displaced by an inhibitor. J. Med. Chem. *44*, 2928–2932.

